Applied Nanoscience (2023) 13:1495–1506
https://doi.org/10.1007/s13204-021-02056-3

ORIGINAL ARTICLE

# Ag-loaded and Pd-loaded ZnO nanofiber membranes: preparation via electrospinning and application in photocatalytic antibacterial and dye degradation

Xian-bing Zhang[1] · Ya-ping Hu[1] · Wei Yang[1] · Ming-bao Feng[2]

Received: 27 April 2021 / Accepted: 28 August 2021 / Published online: 13 September 2021


## Abstract

For the efficient disposal of organic pollutants and *Escherichia coli* (*E. coli*) in water, Ag-loaded and Pd-loaded ZnO nanofibers (NFs) were prepared through electrospinning (e-spin), followed by the alcohol-thermal method. The NFs were prepared in membrane form to promote their separation, recovery, and reuse in practical applications. The complete decolorizations of three types of dyes (i.e., azo, triarylmethane, and heterocyclic dyes) were observed when the Ag-loaded or Pd-loaded ZnO nanofiber membrane (NFM) was first applied as photocatalyst under 30-min UV irradiation. The characterization of the catalysts and the decolorization performance of dyes both demonstrated that the optimal loading rates of Ag and Pd were 12% and 6%, respectively. Moreover, the 12%-Ag/ZnO NFM displayed excellent recyclability over five cycles than the 6%-Pd/ZnO NFM. The *E. coli* disinfection test demonstrated that the photocatalytic inactivation rates with the 12%-Pd/ZnO NFM and the 6%-Ag/ZnO NFM were significantly improved under solar or UV irradiation, and hydroxyl radicals (•OH) was primarily responsible for the antibacterial performance. Therefore, the presented 12%-Ag/ZnO NFM and 6%-Pd/ZnO NFM can be used for the efficient photocatalytic treatment of dyes and *E. coli* in water.

**Keywords** Zinc oxide nanofiber membrane · Ag/Pd loading · Photocatalytic activity · Dye decolorization · Antimicrobial activity · Electrospinning

## Introduction

For the safety of human beings and the ecosystem, hazardous organic pollutants and pathogenic microorganisms [such as dyes, pesticides, antibiotics, and *Escherichia coli* (*E. coli*)] in water must be effectively removed before the water is used or discharged (Yar et al. 2017; Nandhini and Muralidharan 2020). Photocatalytic methods are well known for their relatively low cost, low energy consumption, and high efficiency, and they feature a practically advanced oxidation technique for contaminant disposal in water treatment (Liu et al. 2012; Yar et al. 2017). Improving photocatalytic activity by modifying the catalyst has been an active research area in the past decade (Gupta et al. 2020). Researchers have investigated various methods, such as the loading of noble metals, the doping of transition metals and non-metals (Sehar et al. 2019; Vaiano et al. 2019Sonaimuthu et al. 2020), and the formation of composite photocatalysts using different semiconductors to enhance the photocatalytic activity of nanocatalysts (Ferrone et al. 2019).

Research on photocatalytic nanomaterials for disinfection and organic pollutant degradation via photocatalysis is gradually increasing. Such materials include titanium dioxide ($TiO_2$), bismuth series (BI system), silicon dioxide ($SiO_2$), tungsten trioxide ($WO_3$), and zinc oxide (ZnO) (Venkatesha et al. 2012; Lucía et al. 2012; Hajjaji et al. 2018; Hu et al. 2018; Jayaraj and Thangadurai 2018, 2019; Jaffari et al. 2019; Lee et al. 2019; Panchal et al. 2020; Yin et al. 2020). In this study, ZnO was used as a photocatalyst because its band structure is similar to that of $TiO_2$, but ZnO has higher photocatalytic efficiency and quantum efficiency than $TiO_2$

✉ Xian-bing Zhang
zhangxb11@qq.com

✉ Wei Yang
cqjtuyw@qq.com

[1] Chongqing Key Laboratory of Ecological Waterway, National Inland Waterway Regulation Engineering Research Center, Chongqing Jiaotong University, Chongqing 400074, China

[2] College of Environment and Ecology, Xiamen University, Xiamen 361102, China

in the degradation of organic pollutants (Chen et al. 2019). The easily available ZnO is characterized by large specific surface area and abundant photocatalytic active sites. Moreover, it has the advantages of diversified preparation process, controllable production, low cost, high degradation efficiency, and wide application range. It is a suitable choice for antibacterial materials and organic pollutants degradation in water treatment (Martinez-Carmona et al. 2018; Quek et al. 2018; Ferrone et al. 2019; Salah et al. 2019).

Despite these excellent properties, ZnO also has some limitations, such as high recombination rate and poor photocatalytic activity. Doping some metals (such as Fe, Ag, Ni, Co, Mn, and Cu) into ZnO can significantly improve its photocatalytic efficiency (Younis et al. 2016; Nigussie et al. 2018a,b; Younis et al. 2018; Beura et al. 2018a; Qi et al. 2020; Bian et al. 2020). Ag/ZnO nanostructures in various shapes (nanoparticles, micro/nanoflowers, hybrid nanostructures, hierarchically structures, etc.) were obtained due to high photocatalytic and antimicrobial performance (Hajjaji et al. 2018; Rosalin et al. 2018; Nigussie et al. 2018a,b; Quek et al. 2018; Bian et al. 2020). Nevertheless, the separation, recovery, and reuse of the nanosized catalyst particulates pose a key obstacle to practical applications (Han et al. 2009; Menard et al. 2011). Electrospinning (e-spin) is the most adoptable and efficient method of making nanoparticles into nanofibers (NFs) to overcome the above obstacles (Moheman et al. 2016; Gupta et al. 2019; Filip and Peer 2019). In addition, e-spin is the most effective method adopted for the large-scale preparation of NFs, as it is easy to handle and cost effective; consumes less solution; enables fiber diameter control; and characterized by simple operation, reproducible production, and technical advances (scale-up process) (Thenmozhi et al. 2017; Sehar et al. 2019). However, the majority of nanofiber membranes (NFM) preparation requires harsh environmental conditions, which hinders the engineering application of this technology.

Taking all the advantages of loading noble metals, e-spin ZnO NFs, and membrane materials, the newly designed Ag/ZnO and Pd/ZnO NFMs were attempted to be prepared in normal laboratory conditions. The application potential of synthesized NFMs for photocatalytic disinfection and dye degradation were estimated. Here, Ag is the commonly used noble metal with broad application, while Pd is adopted as the comparison metal to check its photocatalytic performance. *E. coli* was chosen as the target microorganism because it is widely distributed in water bodies, has pathogenic effects, and is an important indicator for evaluating the effectiveness of water treatment (Lam et al. 2018). We separately loaded Ag and Pd on ZnO NFs via the alcohol-thermal method, and the photocatalytic treatment efficiency was greatly improved. The degradation ability of methylene orange (MO) by Ag-loaded and Pd-loaded ZnO NFMs and the optimal noble metal loading amount were studied. The effects of pH, initial MO concentration, and original ZnO usage amount on the MO decolorization performance, and the photocatalytic antibacterial properties of Ag-loaded and Pd-loaded ZnO NFMs were assessed. Both solar simulator irradiation and UV irradiation were adopted to compare the disinfection efficiencies of Ag-loaded and Pd-loaded ZnO NFMs.

## Materials and experimental section

### Materials

Analytical-grade reagents including ethanol glycol (EG), dimethylformamide (DMF), $Zn(AC)_2{\cdot}2H_2O$, MO, malachite green (MG), methylene blue (MB), phosphate buffer solution (PBS, pH 7.2), polyvinylpyrrolidone (PVP, MW = 1.3 million), dimethyl sulfoxide (DMSO), NaOH, and HCl were obtained from Sinopharm Chemical Reagent Co., Ltd. (Shanghai, China). Other reagents such as ethylene glycol (≥ 99.8%), $AgNO_3$ solution (≥ 2.5% (w/v) in $H_2O$), and $PdCl_2$ solution (5 wt% in 10 wt% HCl), and *E. coli* ATCC25922 (standard quality control strain of *Escherichia coli*) were purchased from Aladdin Bio-Chem Technology Co., Ltd. (Shanghai, China).

### Preparation of ZnO NFs

Zinc oxide NFs were prepared in the library with a temperature of 20 °C and humidity of 40% (Pascariu and Homocianu 2019). The main procedures to prepare ZnO NFs include the precursor solution preparation, fiber e-spin, and calcination. Briefly, a solution containing 8 mL DMF, 1.12 g PVP, and 2.5 g $Zn(AC)_2{\cdot}2H_2O$ was well mixed before use. The e-spin fiber-making was operated under a high-voltage direct current of 18 kV, a receiving distance of 13 cm, and a solution outlet speed of 0.5 mL/h. The fibers were collected on an aluminum foil collector and left overnight in air for complete hydrolysis. The ZnO NFs were then calcined in the air at 550 °C for 30 min (See more details in Text S1 and Figure S1).

### Preparation of Ag/ZnO, Pd/ZnO NFM

The Ag-loaded and Pd-loaded ZnO NFMs were prepared via the alcohol-thermal method with a thermostatic magnetic stirrer (DF101s, Shanghai Lichen-Bx Instrument Tech. Co., Ltd., Shanghai, China). First, 100 mg ZnO NFs and 20 mL EG were added into a four-neck flask and stirred at 30 rpm. Then, the solution in the flask was heated to 170 °C, and the temperature was maintained for 30 min. Afterward, PVP solution (100 mg PVP with a MW of 1.3 million was added into 5 mL EG solution and stirred for 15 min) and $AgNO_3$

or PdCl solution (prepared by adding a specific amount of $AgNO_3$ or PdCl into 5 mL EG solution and stirring for 15 min) were slowly added to the four-neck flask through its two inlets, and the mixed solution was heated at 170 °C for another 20 min. The four-neck flask was then cooled to room temperature in a dryer. The cooled solution was filtered through a 0.45 µm filter with a vacuum filtration system (VF204A, Sciencetool Technology Co., Ltd., Shanghai, China). After filtration, the residual PVP and EG on the Ag-coated and Pd-coated ZnO NFMs were removed by washing with ethanol and deionized water five times. Then, the above NFMs were air-dried for 2 h and then physically compacted in a muffle furnace (SX-ES02102, Shuiliuxing Technology Co., Ltd., Nanchang, Jiangxi) at 100 °C for 12 h and subsequently stored in a desiccator for later use. The schematic diagrams of the Ag- and Pd-loaded ZnO NFMs are shown in Fig. 1. For comparison, 100 mg commercial P25 and 100 mg pure $TiO_2$ particles were also used to prepare an NFM with the same method as described above.

As shown in Fig. 1, the Ag/ZnO NFM and Pd/ZnO NFM consisted of two layers: the supporting layer of PE filter and the functional layer of Ag- or Pd-loaded ZnO NFs. When the membrane was submerged in an aqueous solution, the NFM photocatalysts in combination with light irradiation could be adopted for the treatment of organic pollutants and microorganisms.

## Material characterization

The geometric morphologies of the Ag/ZnO NFM and Pd/ZnO NFM were characterized using field-emission scanning electron microscopy (SEM) (Evo18, Carl Zeiss AG, Jena, German) under an accelerating voltage of 30.0 kV. Energy-dispersive X-ray spectroscopy (EDS) was conducted using the EDS system (Xflash6130, Bruker, Beijing, China) attached to the field-emission SEM with carbon tape, and platinum sputtering was adopted for the sample preparations. The X-ray diffractograms (XRD) of the NFMs were carried out with a X-ray powder diffractometer (XPS, D8 advance, Bruker, Beijing, China). The crystal structure of the sample to be measured was determined via scanning analysis at diffraction angles, ranging from 10° to 80°, with an accelerating voltage of 40.0 kV. The diameter of the NFs was analyzed through Image J software.

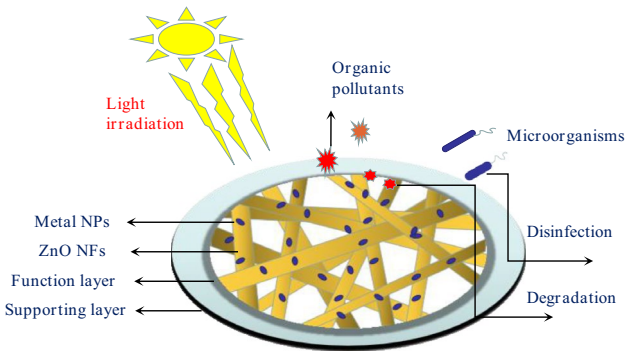


**Fig. 1** Schematic structure of noble metal-loaded ZnO NFM

## Photocatalytic experiments setup for MO degradation

The photodegradation capabilities of the 12%-Ag/ZnO NFM and 6%-Pd/ZnO NFM toward the organic pollutants were evaluated using a model pollutant MO. The dead-end reactor setup was used as shown in Figure S2 with cooling system. At the beginning of each experiment, the Ag/ZnO or Pd/ZnO NFM made from 100 mg ZnO was first placed in the beaker. Then, 100 mL MO solution with an initial concentration of 10 mg/L was poured into the beaker. Thereafter, the mixture was kept in the dark for 1 h to reach the adsorption equilibrium and then kept under light irradiation.

The effect of Ag (4%, 12%, and 20% by weight) or Pb (2%, 6%, and 10%) loading percentage on the decolorization efficiency of MO was assessed, and the optimal loading rate was determined and adopted in the following experiments. Moreover, the effects of the initial MO concentration (10, 15, 20, 25, and 30 mg/L), solution initial pH (3, 4, 5, 7, 9, and 10), and initial weight (ZnO, 0.3, 0.7, and 1.0 mg/mL) used for the ZnO preparation, and the photocatalytic decolorization efficiencies of different dyes (i.e., azo dye MO, triarylmethane dye MG, and heterocyclic dye MB) were studied.

## Photocatalytic disinfection experiments

*E. coli* was chosen as the model pathogen for antibacterial activity tests. It was cultivated in Luria–Bertani nutrient solution at 37 °C for 18 h to obtain the exponential growth phase. The cells were harvested by centrifugation and washed with saline solution (0.9% NaCl) to remove the residual macromolecules. All of the glass apparatuses and solutions used in the experiments were autoclaved at 121 °C for 20 min to ensure sterility. Before the disinfection experiment, 100 mL ultrapure water with an *E. coli* concentration of $(1–2)\times10^6$ CFU/mL was transferred into the 500 mL beaker. The pH value of the solution was adjusted to 7 by HCl/NaOH solution. Then, 100 mg each of the four NFM photocatalysts (P25, ZnO, 12%-Ag/ZnO, 6%-Pd/ZnO) was added into the beaker for each experiment, and the beaker was placed on a magnetic stirrer in a water bath, and the temperature was maintained at 25 °C. The experiments were performed on an aseptic operating table with a UV lamp (UV = 15 MW/cm$^2$, solar simulator = 25 W). During the experiment, 2 mL samples of treated solution were taken out at designed irradiation time intervals. Each sample was

immediately diluted with PBS (pH 7.2), and an appropriate concentration of the sample was spread on nutrient agar and incubated at 37 °C for 24 h. The number of colonies formed was counted to determine the number of viable cells. Control experiments without P25 NFM and with only ZnO NFM were also performed. To investigate the effect of solar irradiation, a control experiment under the same conditions as above but without solar irradiation was performed. Meanwhile, to investigate the complete bacteria inactivation, the same experiments were performed with the extended irradiation time. All of the above experiments were conducted in triplicate.

Hydroxyl radicals (•OH) maybe the major reactive oxygen species (ROS) responsible for the disinfection performance of Ag modified surface leading to bacteria inactivation (Sami et al. 2018). To further improve this assumption, DMSO was used as the •OH scavenger (Salih 2010) and the disinfection performances with the 12%-Ag/ZnO NFM and the 6%-Pd/ZnO NFM were studied in the presence of DMSO at different concentrations (0.0, 10.0, 20.0, and 40.0 mM). Control experiments of DMSO without NFM were also performed.

## Results and discussion

The photocatalyst characterization, photocatalytic potential for disinfection and organic pollutant degradation of Ag-ZnO NFM and Pd-ZnO NFM were studied.

### Characterization of Ag-loaded and Pd-loaded ZnO NFs

The SEM images of ZnO NFs, 12%-Ag/ZnO NFs, and 6%-Pd/ZnO NFs are displayed in Fig. 2. More images of membranes made from different materials are shown in Figure S3. The average diameter of ZnO NFs was 0.65 µm, with a standard deviation of 0.061 (Figure S3a), while the length of the fibers was longer than 50 µm. The polyol (PVP) synthesis is a soft and environmentally friendly fabrication of Ag nanostructures with controlled shapes and properties (Pascariu et al. 2020). In this study, in situ polyol synthesis was used for loading Ag or Pd nanoparticles on ZnO NFs. Figures 2b and c show the SEM images of Ag/ZnO and Pd/ZnO NFs, illustrating that Ag/Pd nanoparticles were uniformly deposited on ZnO NFs. The high-magnification SEM images of Ag/ZnO and Pd/ZnO NFs show that the Ag nanoparticles with size around 50 nm and Pd nanoparticles with size around 6 nm were successfully deposited on the surface of ZnO NFs. The Ag/Pd deposition was further verified via EDS analysis, and the loading amount was estimated as 12 wt% for Ag and 6 wt% for Pd (Figure S4). Compared with the traditional chemical reduction and photodeposition methods, the present polyol synthesis approach does not involve any toxic chemical or UV light, and it can precisely control the growth of Ag/Pd nanoparticles on ZnO NFs (Vaiano et al. 2019; Li et al. 2020).

To further determine the chemical properties of the Ag/ZnO and Pd/ZnO NFs, X-ray diffraction (XRD) was employed. Figure S5 shows that the XRD patterns of pure ZnO NFs, Ag/ZnO NFs, and Pd/ZnO NFs had diffraction peaks related to the (002), (100), (101), (102), (103), (110), (112), (201), and (202) planes of the anatase phase of ZnO, which favors photocatalytic oxidation better than the rutile phase (Mo and Ching1995; van der Meulen et al 2007). In the curves of Ag/ZnO NFs and Pd/ZnO NFs, clear peaks of Ag/Pd (111), (200), and (220) further confirmed that the Ag/Pd nanoparticles were successfully deposited on ZnO NFs.

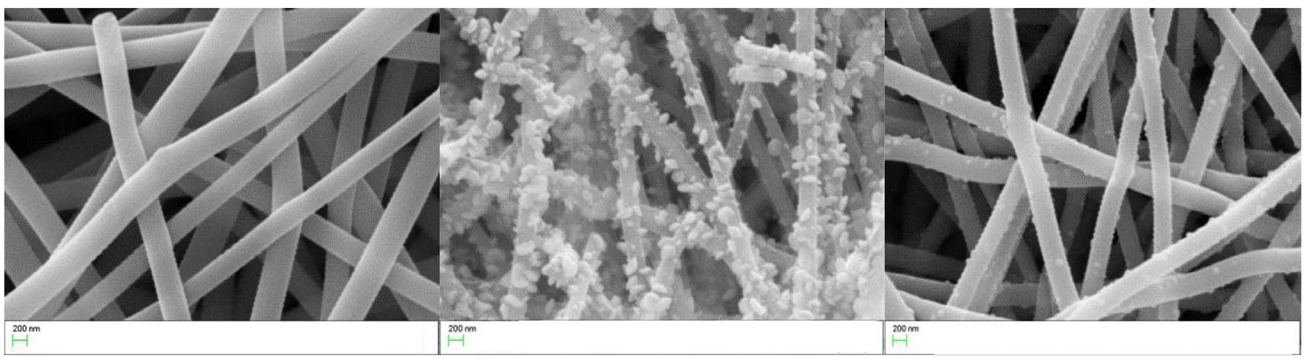


**Fig. 2** SEM images of **a** ZnO NFs, **b** 12%-Ag/ZnO NFs, and **c** 6%-Pd/ZnO NFs (12%-Ag/ZnO represents the system with 12 wt% of silver loaded on ZnO NFM)

## Photocatalytic performance for dye degradation

### MO decolorization under UV irradiation

The photocatalytic decontamination properties of Ag/ZnO NFM and Pd/ZnO NFM were investigated by the examination of organic pollutant MO under solar/UV irradiation. The MO solution exhibited two obvious UV–vis absorption peaks, at 271 nm and 465 nm, which were generated by –N=N– and benzene ring conjugation bond, respectively (Figure S6 and Table S1). Figure 3 shows that MO could be almost completely decolorized after 30 min of photocatalytic treatment by both the 12%-Ag/ZnO NFM and 6%-Pd/ZnO NFM. This degradation performance was further proved by the disappearance of the solution color (Figs. 3c and d). According to Figure S6, the UV–vis absorption peaks at 271 nm and 465 nm also disappeared after 30 min when the 12%-Ag/ZnO NFM and 6%-Pd/ZnO NFM were used as the photocatalysts. The decolorization efficiencies of MO were much lower in the other experiments. For example, MO could not be degraded without catalyst or light irradiation, and nearly 30%, 46%, and 62% MO decolorization rates were observed after 30 min under UV irradiation alone, UV with P25, and UV with ZnO, respectively. For 4%-, 12%-, and 20%-Ag/ZnO NFMs combined with 30 min UV irradiation, 95%, 100%, and 97% MO decolorization rates were observed, respectively. As for 4%-, 12%-, and 20%-Pd/ZnO NFMs combined with 30 min UV irradiation, 95%, 100%, and 97% decolorization rates of MO were individually observed.

The data could also be satisfactorily analyzed using the first-order kinetic equation to obtain the rate constants. In the presence of P25 or ZnO NFM under UV irradiation, comparable kinetic rate constants were observed (i.e., 0.105 $min^{-1}$

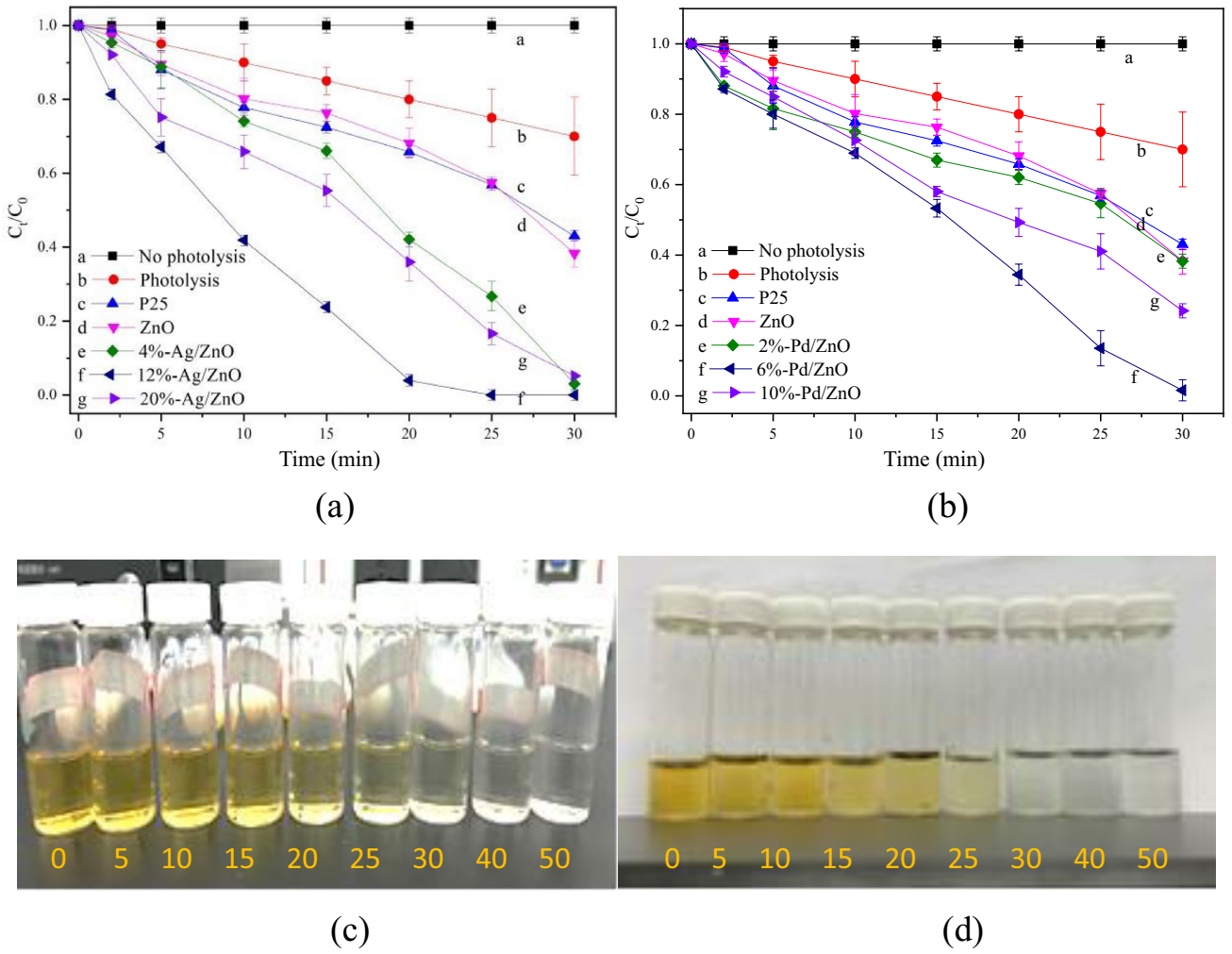


**Fig. 3** UV photocatalytic discoloration of MO using different catalysts: **a** Ag/ZnO NFM and **b** Pd/ZnO NFM; **c** MO decolorization versus irradiation time in 12%-Ag/ZnO NFM system; and **d** MO decolorization versus irradiation time in 6%-Pd/ZnO NFM system. (Experimental conditions: $[MO]_0 = 10$ mg/L, [Catalyst] = 1 g $L^{-1}$, $pH_0 = 7.0$, $T = 25$ °C, UV lamp = 300 W)

and 0.104 $min^{-1}$, respectively). In the presence of Ag/ZnO or Pd/ZnO NM, the MO decolorization rate could be significantly improved (Fig. 3 and Table 1). The MO decolorization rate constants were 0.368 $min^{-1}$ and 0.231 $min^{-1}$ when 12%-Ag/ZnO and 6%-Pd/ZnO were adopted, respectively. From the SEM images and MO decolorization results, the optimal loading amounts of Ag and Pd on the ZnO NF surface were 12% and 6%, respectively.

### Influence of initial pH

According to the literature, pH value is the major factor influencing the rate of the photocatalytic process (Lachheb et al. 2002; Guettai and Amar 2005). Therefore, experiments were performed to determine the optimal pH for MO decolorization. In all the experiments, the pH was adjusted by adding an appropriate amount of NaOH or $H_2SO_4$ solution. The results are presented in Figure S7.

The better results were obtained in acidic solution, and the best result was observed when the initial pH was 4. However, the MO degradation rate at the initial pH of 3 was the same as that at the initial pH of 5. In addition, MO could be completely decolorized in the 12%-Ag/ZnO NM degradation system within 35 min when the initial solution pH was 3–10 (Figure S7). Other researchers also found the same results when Cu–$TiO_2$-based NFs were adopted as a photocatalyst for virus removal (Zhang et al 2018). The possible explanation for these results is pH can influence the adsorption of dye molecules onto the catalytic material surface, which is an important step for the photooxidation to occur. Thus, the electron transfer efficiency will be decreased at pH higher than 9 or lower than 4. For both the 12%-Ag/ZnO and 6%-Pd/ZnO photocatalytic systems, the best treatment performance was at an initial pH of 4.

### Influence of original ZnO amount in catalyst preparation

As discussed in Sect. 3.2.1, the optimal loading rates (by weight) of Ag and Pd on ZnO NFs were 12% and 6%, respectively. The catalyst dosage is another important factor that influences the photocatalytic efficiency. To determine the optimal amount of photocatalyst, the effect of catalyst dosage, measured by the original amount of ZnO used (0.3, 0.7, and 1.0 mg/mL ZnO), on the decolorization performance of MO were studied at an initial pH of 7, and the results are shown in Figure S8. It should be noted that more catalysts could be produced with a constant loading rate (Ag, 12%; Pd, 6%) when more original ZnO were used.

Figure S8 shows that the decolorization rate of MO increased significantly with increasing amounts of the original ZnO usage from 0.3 to 0.7 mg/mL. However, the decolorization rate of MO was little increased with further increase in the original ZnO amount from 0.7 to 1.0 mg/mL. As the catalyst dosage increased, more active sites could be available on the catalyst surface, and more oxidants could be produced, thus increasing the photodegradation performance (Lee et al. 2015). However, the usage of light may play a dominate role in the further enhanced treatment efficiency, demonstrated by the increased decolorization rate when a sufficient amount of photocatalysts was adopted. In the present study, the light scattering due to the material aggregation was unlikely to occur because noble metal (Ag or Pd) was uniformly loaded on the surface of ZnO NFs and further transformed it into a membrane.

### Effect of initial concentration of MO

The effect of the initial MO concentration in water on the photocatalytic degradation performance was examined, as the concentrations of the characteristic dyes in water vary greatly (Ray 1999; Guettai and Amar 2005). Thus, the photocatalytic decomposition of MO using the 12%-Ag/ZnO NFM or 6%-Pd/ZnO NFM made from 100 mg ZnO was studied by varying the initial MO concentrations from 10 to 30 mg/L at pH = 7. The relationship between the MO concentration and time in the 12%-Ag/ZnO NFM or 6%-Pd/ZnO NFM photocatalytic system is illustrated in Figure S9.

Figure S9 shows that MO could be efficiently degraded by both the 12%-Ag/ZnO NFM and 6%-Pd/ZnO NFM systems, but the time needed for complete decolorization increased significantly with the increased initial concentrations of MO. In the 12%-Ag/ZnO NFM system, the times needed for the complete decolorization of 10, 15, 20, 25, and 30 mg/L MO were 30, 70, 105, 145, and 180 min, respectively. In the 6%-Pd/ZnO NFM system, the corresponding times were prolonged to 40, 80, 110, 175, and 200 min, respectively.

As mentioned by other researchers (Houas et al.2001; Marcì et al. 2003; Guettai and Amar 2005), the requirement of catalyst surface needed for the photodegradation also increases to produce more oxidizing species as the initial concentrations of the dye increases. In the current study, the screening effect of UV at a high dye concentration was

**Table 1** The first-order kinetic rate constants of Ag-loaded and Pd-loaded ZnO NF membranes for MO degradation

| Catalyst | ZnO | P25 | 4%-Ag/ZnO | 12%-Ag/ZnO | 20%-Ag/ZnO |
|---|---|---|---|---|---|
| $k$ ($min^{-1}$) | 0.104 ± 0.015 | 0.105 ± 0.010 | 0.195 ± 0.042 | 0.368 ± 0.059 | 0.241 ± 0.040 |
| Catalyst | **ZnO** | **P25** | **2%-Pd/ZnO** | **6%-Pd/ZnO** | **10%- Pd/ZnO** |
| $k$ ($min^{-1}$) | 0.104 ± 0.015 | 0.105 ± 0.010 | 0.159 ± 0.020 | 0.231 ± 0.044 | 0.158 ± 0.017 |

reduced and more active sites will be covered by dye ions when the initial dye concentration increased. Then, the photogeneration of holes or •OH radicals on the catalyst surface will reduced, which ultimately lead to the decreasing of the catalytic reaction efficiency (Konstantinou and Albanis 2004).

### The performance of different types of dyes

From the above experimental results, the 12%-Ag/ZnO NFM and 6%-Pd/ZnO NFM were effective for the photodegradation of the azo dye MO. However, further study is needed to determine whether the present NFM photocatalysts are still effective for the degradation of other types of dyes. Therefore, except the azo dye MO, the other commonly used types of dyes, such as the triarylmethane dye MG and the heterocyclic dye MB (Liu et al. 2020), were adopted to study the efficiency of the present photocatalysts. More details on the three types of dyes are presented in Table S1.

The original concentrations and pH of MG and MB solutions were 10 mg/L and 7.0, respectively. Before each experiment, 100 mL of dye solution was separately mixed with ZnO, 12%-Ag/ZnO NFM, and 6%-Pd/ZnO NFM, and then the mixture was kept in the dark for 10 h to obtain the absorption equilibrium. Afterward, the dye solution was subjected to photocatalytic decolorization experiments under UV irradiation as described in Sect. 2.5. The photocatalytic decolorization results of MG and MB solutions with different catalysts are depicted in Figure S10.

As shown in Figure S10, the MG and MB solutions could be effectively decolorized as MO within 40 min when 12%-Ag/ZnO NFM and 6%-Pd/ZnO NFM were used as the photocatalysts. The disappeared color and peak wavelength of MG and MB solutions both demonstrated the high decolorization efficiencies of the present catalysts. Furthermore, the 12%-Ag/ZnO NFM still had the best photocatalytic performance, and the 6%-Pd/ZnO NFM was better than the ZnO NFM. The above results demonstrated that the 12%-Ag/ZnO NFM and 6%-Pd/ZnO NFM were effective for the photo-decolorization of azo, triarylmethane, and heterocyclic dyes in water.

### Stability and reusability of the photocatalysts

The stability of the photocatalyst is an important factor for the engineering application of photocatalytic technology. Therefore, the stability and repeatability of the 12%-Ag/ZnO NFM and 6%-Pd/ZnO NFM were investigated according to the previous publications (Singh and Dhaliwal 2020; Ng et al. 2016; Zhang et al. 2017). MO solution (as detailed in Sect. 2.5) was used to perform repeatability experiments. As shown in Fig. 4, the MO solution was fully decolorized by the 12%-Ag/ZnO NFM with UV irradiation in 30 min after five cycles. That means the 12%-Ag/ZnO NFM was very stable in the present solution. In contrast, double time was needed for complete decolorization of MO when the 6%-Pd/ZnO NFM was adopted (as shown in Fig. 4b).

## Photocatalytic disinfection

### Disinfection under UV irradiation

The photocatalytic inactivation of *E. coli* using different photocatalysts under different conditions is demonstrated in Fig. 5. The first-order kinetic equation was used to calculate the inactivation rates ($k$) according to the disinfection results (Wang et al. 2018). As shown in Fig. 5a, 99% of *E. coli* was disinfected after 30 min of UV irradiation with or without NFM, which means that the UV irradiation itself had an

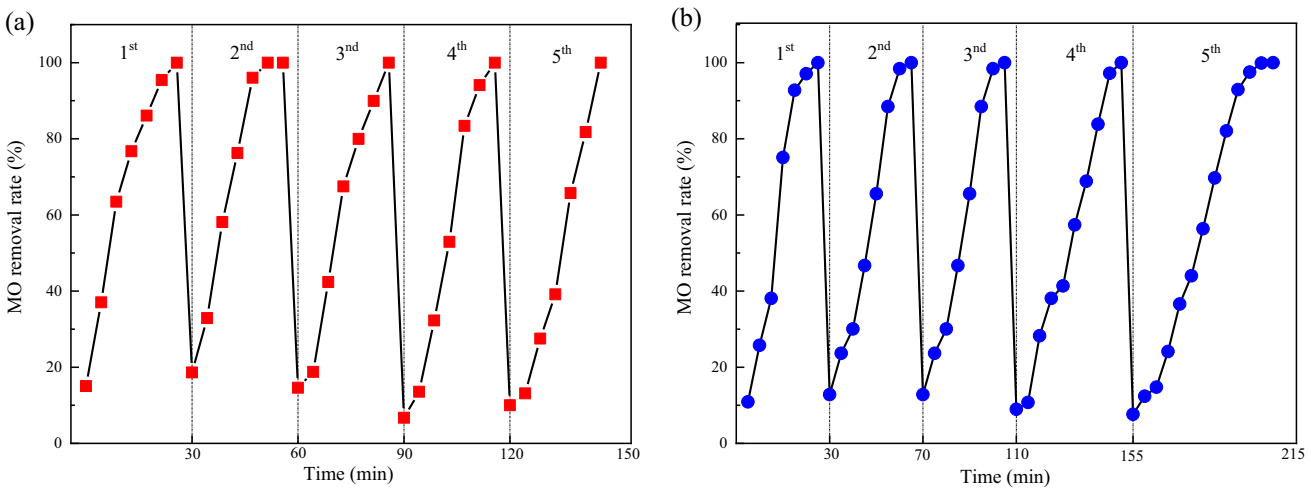


**Fig. 4** Recyclability tests on photocatalytic degradation of MO with **a** 12%-Ag/ZnO NFM and **b** 6%-Pd/ZnO NFM. (Experimental conditions: $[MO]_0 = 10$ mg/L, [Catalyst] = 1 g $L^{-1}$, $pH_0 = 7.0$, $T = 25$ °C, UV lamp = 300 W)

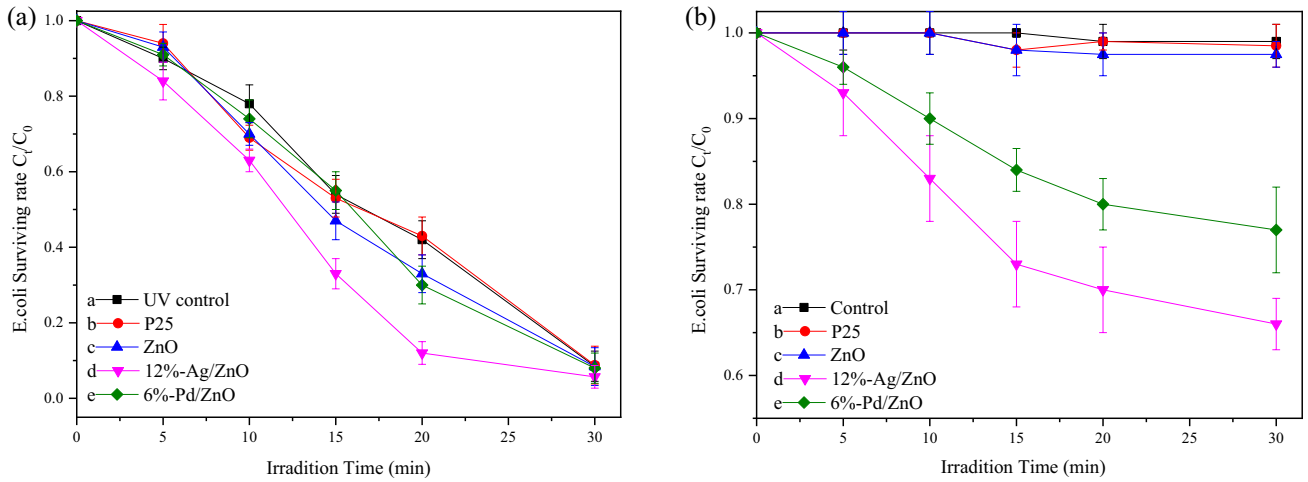


**Fig. 5** Photocatalytic disinfection of *E. coli* with different membranes under **a** UV and **b** solar irradiation. (Experimental conditions: [*E. coli*]$_0 = (1-2)\times10^6$ CFU/mL, [Catalyst] = 1 g L$^{-1}$, pH$_0$ = 7.0, $T$ = 25 °C, UV = 15 mw/cm$^2$, solar simulator = 25 W)

effective disinfection performance for *E. coli*. Comparatively, the inactivation rates with the 12%-Pd/ZnO NFM and the 6%-Ag/ZnO NFM were greatly improved. For example, the disinfection rates obtained by different materials were as follows: UV alone: 0.079 min$^{-1}$, P25 NFM: 0.080 min$^{-1}$, ZnO NFM: 0.083 min$^{-1}$, 12%-Pd/ZnO NFM: 0.104 min$^{-1}$, and 6%-Ag/ZnO NFM: 0.081 min$^{-1}$.

When cationic dopant is added to ZnO, the commonly accepted mechanism was as follows (Lee et al. 2016):

$$\mathrm{ZnO} + h\nu \rightarrow \mathrm{ZnO}\left(e^-_{\mathrm{CB}} + h^+_{vb}\right), \quad (1)$$

$$e^-_{\mathrm{CB}} + \mathrm{M}^{\mathrm{n+}} \rightarrow \mathrm{M}^{(\mathrm{n-1})+}, \quad (2)$$

$$\mathrm{O_2} + \mathrm{M}^{(\mathrm{n-1})+} \rightarrow \cdot\mathrm{O}^-_2 + \mathrm{M}^{\mathrm{n+}}, \quad (3)$$

$$\mathrm{O}\left(h^+_{vb}\right) + \mathrm{OH}^- \rightarrow \mathrm{ZnO} + \bullet\mathrm{C} \quad (4)$$

$$\bullet\mathrm{OH} + \text{ organic contaminate } \rightarrow \text{degradation products } + \mathrm{CO_2} + \mathrm{H_2O}. \quad (5)$$

## Disinfection under solar irradiation

As control, solar simulator irradiation was performed in the absence of photocatalyst. Figure 5b indicates that 99.0% of the bacteria survived after 30 min of solar irradiation. These results reveal that the solar irradiation intensity had no significant antibacterial effect on *E. coli* within 30 min. The antibacterial activities of the 12%-Ag/ZnO NFM and 6%-Pd/ZnO NFM without solar irradiation were also investigated for comparison. Both P25 NFM and ZnO NFM showed no antibacterial capability in the absence of solar irradiation, implying that ZnO NFM was not toxic to the bacteria (Fig. 5b). The survival rate of *E. coli* in the 12%-Ag/ZnO NFM solar irradiation system was 10% higher than that in the 6%-Pd/ZnO NFM solar irradiation system. Comparing the results in Figs. 5a and b, it can be concluded that when the 12%-Ag/ZnO and 6%-Pd/ZnO NFMs were adopted as the photocatalysts, the disinfection efficiency under UV irradiation was 20% higher than that under solar irradiation, and the former catalyst had better disinfection performance. According to Table S2, the photocatalytic performance of 12%-Ag/ZnO and 6%-Pd/ZnO NFMs in this study is better or comparable to other reported results with different type of catalysts. The present of the dopants (such as Ag, Pd, Cu, et al.) could increase the specific surface area of ZnO, reduce the resistivity of ZnO, and also reduce the activation energy in the photocatalytic activity (Xia et al. 2016). The above reasons lead to the better photocatalytic performance of Ag-loaded or Pd-loaded NFM than that of ZnO NFM. Furthermore, lower band gap energy value and higher solubility make the Ag-loaded NFM have better photocatalytic performance than Pd-loaded NFM.

## ·OH trapping test

Generally, antibacterial materials made from metal inorganic nanocomposites mainly have two antibacterial mechanisms: (1) photocatalytic antibacterial mechanism and (2) metal-contact antibacterial mechanism (Ashebir et al. 2018). To distinguish which of these mechanisms was dominant in the

materials and the role of ROS (such as $H_2O_2$, •OH, $h^+$, $•O_2^-$) produced during photocatalytic disinfection (Lam et al. 2018; Quek et al. 2018; Jaffari et al. 2019), ROS trapping test was performed. In these experiments, ordinary solar irradiation was adopted to study the antibacterial effect of the self-made catalysts.

As shown in Fig. 6, with the increase in the DMSO concentration, the bacteria survival rate was significantly increased. When 40 mM DMSO was added into the system, the bacteria survival rate almost increased to that of Ag/ZnO (or Pd/ZnO) NFM without solar irradiation (Figs. 6a and b). The control experiment using DMSO (40 mM) in the absence of 12%-Ag/ZnO (or 6%-Pd/ZnO) NFM did not show any significant antibacterial ability. When 0.0, 10.0, 20.0, and 40 mM DMSO were added to the 12%-Ag/ZnO NFM disinfection system with solar irradiation, the *E. coli* survival rates were 66%, 77%, 82%, and 97.5%, respectively. The corresponding survival rates for the 6%-Pd/ZnO NFM disinfection system with solar irradiation were individually measured as 77%, 80%, 97%, and 98%. This indicates that a high yield of •OH was generated in the Ag/ZnO (or 6%-Pd/ZnO) NFM under solar irradiation.

Furthermore, the 12%-Ag/ZnO NFM exhibited a better disinfection performance than the 6%-Pd/ZnO NFM under the current experimental conditions. This can be further confirmed by the *E. coli* survival rates when 20 mM DMSO was adopted in the disinfection systems (Fig. 6). One possible reason for the better disinfection performance is the higher loading amount and activity of 12%-Ag/ZnO than those of 6%-Pd/ZnO NFM, with an assumption that all •OH produced could be completely captured by 20 mM DMSO. If this assumption is true, then less *E. coli* survived when 40 mM DSMO was adopted. Another possible reason is that more •OH was produced in the 12%-Ag/ZnO NFM disinfection system than in the 6%-Pd/ZnO system because silver particles have a higher activity, so that more •OH will be produced under photocatalysis. When the DMSO dosage was 40 mM, the 12%-Ag/ZnO NFM disinfection system almost lost its antibacterial effect, which proves that •OH was primarily responsible for the photocatalytic disinfection in 12%-Ag/ZnO (or 6%-Pd/ZnO) NFM under solar irradiation.

## Antibacterial activity by Kirby-Bauer approach

To investigate the intrinsic chemical antibacterial strength of the Ag-loaded and Pd-loaded ZnO NFMs (cut into 1-cm square blocks), a standard Kirby-Bauer approach was applied. *E. coli* was inoculated with Ag/ZnO or Ag/ZnO NFM on the agar plates for 24 h. ZnO NFM was also investigated for comparison. The details of the experimental procedure have been reported by Gupta (Gupta et al. 2020), and the results are shown in Fig. 7. An antibacterial zone existed around 12%-Ag/ZnO NFM and 6%-Pd/ZnO NFM, but no inhibition zone existed around the ZnO NFM. The inhibition zones of 12%-Ag/ZnO and 6%-Pd/ZnO were both increased by more than 3 mm after 16 h of incubation (Fig. 7).

To further confirm that this antibacterial effect was induced by the self-made NFM rather than the supporting layer, the above experiments were repeated using only the functional layer or the supporting layer. The results are shown in Figures S11 and S12. After 16 h of incubation, no inhibition zone was observed when only the supporting layer was adopted. In contrast, both the functional layers of 12%-Ag/ZnO and 6%-Pd/ZnO NFM had inhibition

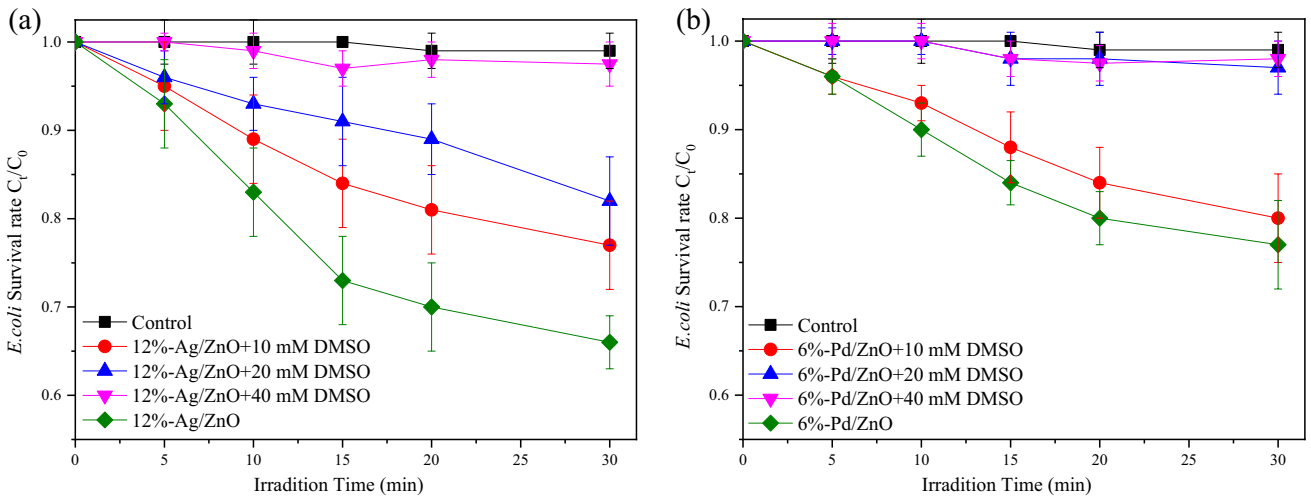


**Fig. 6** Effect of DMSO concentrations on the photocatalytic disinfection of *E. coli* under solar irradiation: **a** 12%-Ag/ZnO NFM; **b** 6%-Pd/ZnO NFM. (Experimental conditions: $[E.\ coli]_0 = (1-2) \times 10^6$ CFU/mL, [Catalyst] = 1 g $L^{-1}$, $pH_0 = 7.0$, $T = 25$ °C, solar simulator = 25 W)

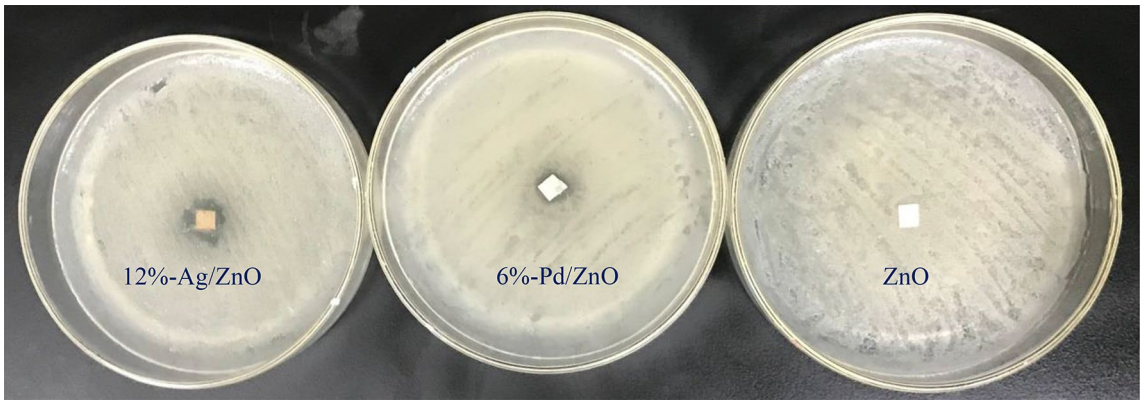


**Fig. 7** Antibacterial test for different NFM materials. (Experimental conditions: target bacterial was *E. coli*, $T = 37$ °C, incubation time was 16 h, the materials were cut into ~ 1 cm square block)

zones, and the inhibition area increased as the incubation time was prolonged from 16 to 48 h (Figure S11 and Figure S12).

Furthermore, the NFs with Ag or Pd metal particles in contact with ZnO reduce the bandgap energy by increasing the $e^- - h^+$ charge separation time and thus result in a higher antibacterial activity than the NFs containing only ZnO (Gupta et al. 2020; Salih 2010). It has been reported (Nigussie et al. 2018a,b) that noble metal ions inhibit the enzymes for ATP hydrolysis and expression of ribosomal proteins by hindering the DNA replication of bacteria. Lam's team confirmed that Ag/ZnO micro/nanoflowers can severely cause the bacterial cells ruptured, leading to leakage of membrane integrities such as nucleic acids and proteins and consequently led to cell death (Lam et al. 2018). The valence band electrons in these nanoparticle materials (NPM) under sunlight with the photons of energy greater than or equal to ZnO band gap electrons can be excited to the conduction band producing an equal number of holes in the valence band, simultaneously. Because the conduction band energy level of ZnO NPM is higher than that of the intraband state of Ag-loaded ZnO and Pd-loaded ZnO NFM, electrons can flow from ZnO to Ag-loaded/Pd-loaded NFM (Yamanaka et al. 2005; Ashebir et al. 2018). So, oxygen vacancy defects and Ag/Pd on the surface of ZnO NFM trap electrons and prevent the recombination of $e^-_{CB}$ pairs. Here, the intraband state of Ag maybe lower than Pd; this is why Ag-loaded ZnO NFM has a higher photocatalytic efficiency than Pd-loaded ZnO NFM (Chen et al. 2008). These results demonstrate that ZnO NFM alone had no significant antibacterial effect, while the noble metal-loaded ZnO NFM had a significant antibacterial effect, and the 12%-Ag/ZnO NFM had better antibacterial performance than the 6%-Pd/ZnO NFM.

## Conclusions

In this study, Ag-loaded and Pd-loaded ZnO NFMs were successfully fabricated by e-spin, followed by the alcohol-thermal method. The SEM, EDS, and XRD tests proved that the Ag and Pd noble metal particles were uniformly deposited on ZnO NFs, and the optimal loading rates of Ag and Pd were 12% and 6% (by weight), respectively. The 12% Ag and 6% Pd on ZnO were quite a lot for the best performance due to the difference of atomic radius, molecular weight and particle size after loading between Ag and Pd.

Besides, 10 mg/L MO solution could be completely decolorized when both the 12%-Ag/ZnO NFM and 6%-Pd/ZnO NFM were used as the photocatalysts with 30 min of UV irradiation. Besides the azo dye MO, MG and MB could also be effectively decolorized in 12%-Ag/ZnO NFM and 6%-Pd/ZnO NFM photocatalytic systems. The solution pH, catalyst usage, and dye concentration all affected the photocatalytic treatment efficiency. The better decolorization results were observed in acidic solution with lower dye concentration and suitable catalyst dosage, and the best decolorization result was observed when the initial pH was 4 in both the 12%-Ag/ZnO NFM and 6%-Pd/ZnO NFM photocatalytic systems.

Moreover, ultraviolet irradiation used alone had a strong *E. coli* disinfection effect, while the photocatalytic inactivation rates with the 12%-Pd/ZnO NFM and 6%-Ag/ZnO NFM were significantly improved under solar and UV irradiation. In addition, the •OH scavenger test demonstrated that •OH was primarily responsible for the photocatalytic disinfection in the 12%-Ag/ZnO (or 6%-Pd/ZnO) NFM under solar irradiation. The antibacterial activity determined by the Kirby–Bauer approach revealed that

ZnO NFM alone had no significant antibacterial effect, while the noble metal-loaded ZnO NFM had a significant antibacterial effect, and the 12%-Ag/ZnO NFM had better antibacterial performance than the 6%-Pd/ZnO NFM.

Overall, the present self-made Ag-loaded and Pd-loaded ZnO NFMs can be adopted as effective photocatalysts for dye decolorization and *E. coli* disinfection in water treatment.

**Supplementary Information** The online version contains supplementary material available at https://doi.org/10.1007/s13204-021-02056-3.

**Acknowledgements** Chongqing Human Resources and Social Security Bureau Innovation Program for Returned Overseas Researchers financially supported this work. In addition, we thank Virender K. Sharma for the improvement of the manuscript structure and illustration.

## Declarations

**Conflict of interest** All authors declare that there is no conflict of interest.

## References

Ashebir ME, Tesfamariam GM, Nigussie GY, Gebreab TW (2018) Structural, optical, and photocatalytic activities of Ag-doped and Mn-doped ZnO nanoparticles. J Nanomater 2018:9425938

Bandara PC, Tapire E, Peña-Bahamonde N, Rodrigues DF (2019) Impact of water chemistry, shelf-life, and regeneration in the removal of different chemical and biological contaminants in water by a model polymeric graphene oxide nanocomposite membrane coating. J Water Process Eng 32:100967

Beura R, Pachaiappan R, Thangadurai P (2018a) A detailed study on $Sn^{4+}$ doped ZnO for enhanced photocatalytic degradation. Appl Surf Sci 433:887–898

Beura R, Pachaiappan R, Thangadurai P (2018b) Effect of Sn doping in ZnO on the photocatalytic activity of ZnO-graphene nanocomposite with improved activity. J Environ Chem Eng 6:5087–5100

Bian H, Zhang Z, Xu X, Gao Y, Wang T (2020) Photocatalytic activity of Ag/ZnO/AgO/$TiO_2$ composite. Phys E 124:114236–114241

Chen T, Zheng Y, Lin JM, Chen G (2008) Study on the photocatalytic degradation of methyl orange in water using Ag/ZnO as catalyst by liquid chromatography electrospray ionization ion-trap mass spectrometry. J Am Soc Mass Spectrom 19:997–1003

Chen S, Liu F, Xu M, Yan J, Liu C (2019) First-principles calculations and experimental investigation on SnO2@ZnO heterojunction photocatalyst with enhanced photocatalytic performance. J Colloid Interface Sci 553:613–621

Ferrone E, Araneo R, Notargiacomo A, Pea M, Rinaldi A (2019) ZnO Nanostructures and electrospun ZnO-polymeric hybrid nanomaterials in biomedical, health, and sustainability applications. Nanomaterials (basel, Switzerland) 9:1499–1532

Filip P, Peer P (2019) Characterization of poly (ethylene oxide) nanofibers-mutual relations between mean diameter of electrospun nanofibers and solution characteristics. Process 7(12):948

Guettai N, Amar HA (2005) Photocatalytic oxidation of methyl orange in presence of titanium dioxide in aqueous suspension. Part I: Parametric Study. Desalination 185:427–437

Gupta A, Gurunathan P, Ramesha K, Singh M, Dhakate SR (2019) Effect of heat treatment temperature on energy storage performance of PAN co-MMA based carbon nanofibers as freestanding lithium ion batteries anode. Energy Storage 1:16669–16677

Gupta A, Khosla N, Govindasamy V, Saini A, Annapurna K, Dhakate SR (2020) Trimetallic composite nanofibers for antibacterial and photocatalytic dye degradation of mixed dye water. Appl Nanosci 10:4191–4205

Hajjaji A, Elabidi M, Trabelsi K (2018) Bacterial adhesion and inactivation on Ag decorated TiO-nanotubes under visible light effect of the nanotubes geometry on the photocatalytic activity. Colloid Surf B 170:92–98

Han F, Kambala VSR, Srinivasan M, Rajarathnam D, Naidu R (2009) Tailored titanium dioxide photocatalysts for the degradation of organic dyes in wastewater treatment: a review. Appl Catal A 359:124–148

Houas A, Lachheb H, Ksibi M, Elaloui E, Guillard C, Herrmann J (2001) Photocatalytic degradation pathway of methylene blue in water. Appl Catal B 31:145–157

Hu X, Xu P, Gong H, Yin G (2018) Synthesis and characterization of $wo_3$/graphene nanocomposites for enhanced photocatalytic activities by one-step in-situ hydrothermal reaction. Materials 11:147–163

Jaffari ZH, Lam SM, Sin JC, Mohamed AR (2019) Constructing magnetic Pt-loaded $BiFeO_3$ nanocomposite for boosted visible light photocatalytic and antibacterial activities. Environ Sci Pollut Res 26:10204–10218

Jayaraj SK, Thangadurai P (2018) Enhanced visible-light-driven photodegradation of Rh-6G by surface engineered Pd-$V_2O_5$ heterostructure nanorods. J Environ Chem Eng 6:5320–5331

Jayaraj SK, Thangadurai P (2019) Surface engineering of Au decorated $V_2O_5$ nanorods-enhanced photodegradation of Rh-6G under visible light with high cyclability and stability. J Environ Chem Eng 7:103512

Konstantinou IK, Albanis TA (2004) Worldwide occurrence and effects of antifouling paint booster biocides in the aquatic environment: a review. Environ Int 30:235–248

Lachheb H, Puzenat E, Houas A, Ksibi M, Elaloui E, Guillard C, Herrmann JM (2002) Photocatalytic degradation of various types of dyes (Alizarin S, Crocein Orange G, Methyl Red, Congo Red, Methylene Blue) in water by UV-irradiated titania. Appl Catal B 39:75–90

Lam SM, Queka JA, Sinb JC (2018) Mechanistic investigation of visible light responsive Ag/ZnO micro/nanoflowers for enhanced photocatalytic performance and antibacterial activity. J Photochem Photobiol A 353:171–184

Lee KM, Hamid SBA, Lai CW (2015) Multivariate analysis of photocatalytic-mineralization of Eriochrome Black T dye using ZnO catalyst and UV irradiation. Mater Sci Semicond Process 39:40–48

Lee KM, Lai CW, Ngai KS, Juan JC (2016) Recent developments of zinc oxide based photocatalyst in water treatment technology: a review. Water Res 88:428–448

Lee JW, Jang YI, Park WS, Kim SW, Lee BJ (2019) Photocatalytic and pozzolanic properties of Nano-$SiO_2$/$Al_2O_3$-$TiO_2$ powder for functional mortar. Materials (basel) 12:1037–1052

Li H, Wang X, Chen X, Li C, Liang C (2020) A schiff base modified Pd catalyst for selective hydrogenation of 2-Butyne-1,4-diol to 2-Butene-1,4-diol. Catal Lett 150:2150–2157

Liu L, Liu Z, Bai H, Sun DD (2012) Concurrent filtration and solar photocatalytic disinfection/degradation using high-performance Ag/$TiO_2$ nanofiber membrane. Water Res 46:1101–1112

Liu G, Abukhadra MR, El-Sherbeeny AM, Mostafa AM, Elmeligy MA (2020) Insight into the photocatalytic properties of diatomite@Ni/NiO composite for effective photo-degradation of malachite green dye and photo-reduction of Cr (VI) under visible light. J Environ Manag 254:109799.1-109799.10

Lucía DCC, María DCG, Acosta EO, Ginzberg B (2012) Removal of Cr(VI) and humic acid by heterogeneous photocatalysis in a laboratory reactor and a pilot reactor. Ind Eng Chem Res 51:9468–9474

Marcì G, Augugliaro V, Prevot AB, Baiocchi C, Schiavello M (2003) Photocatalytic oxidation of methyl-orange in aqueous suspension: comparison of the performance of different polycrystalline titanium dioxide. Anal Chim 93:639–648

Martinez-Carmona M, Gun'Ko Y, Vallet-Regi M (2018) ZnO nanostructures for drug delivery and theranostic applications. Nanomaterials 8:268–294

Menard A, Drobne D, Jemec A (2011) Ecotoxicity of nanosized $TiO_2$. Rev Vivo Data Environ Pollut 159:677–684

Meulen T, Mattson A, Österlund L (2007) A comparative study of the photocatalytic oxidation of propane on anatase, rutile, and mixed-phase anatase–rutile $TiO_2$ nanoparticles: role of surface intermediates. J Catal 25:131–144

Mo SD, Ching WY (1995) Electronic and optical properties of three phases of titanium dioxide: rutile, anatase, and brookite. Phys Rev B 51:13023

Mohandoss S, Edison TNJI, Atchudan R, Palanisamy S, Prabhu NM, You AANSG, Lee YR (2020) Ultrasonic-assisted efficient synthesis of inclusion complexes of salsalate drug and β-cyclodextrin derivatives for potent biomedical applications. J Mol Liq 319:114368

Moheman A, Alam MS, Gupta A, Dhakate SR, Mohammad A (2016) Fabrication of nanofiber stationary phases from chopped polyacrylonitrile co-polymer microfibers for use in ultrathin layer chromatography of amino acids. RSC Adv 6:90100–90110

Nandhini S, Muralidharan G (2020) Co3S4-CoS/rGO hybrid nanostructure: promising material for high-performance and high-rate capacity supercapacitor. J Solid State Electr 25(2):465–477

Ng TW, Zhang L, Liu HJG, Wong PK (2016) Visible-light-driven photocatalytic inactivation of *Escherichia coli* by magnetic $Fe_2O_3$-AgBr. Water Res 90:111–118

Nigussie GY, Tesfamariam GM, Tegegne BM, Weldemichel YA, Gebremichel GE (2018a) Antibacterial activity of Ag-doped $TiO_2$ and Ag-doped ZnO nanoparticles. Int J Photoenergy. https://doi.org/10.1155/2018/5927485

Nigussie GY, Tesfamariam GM, Tegegne BM, Weldemichel YA, Gebremichel GE (2018b) Antibacterial activity of Ag-doped $TiO_2$ and Ag-doped ZnO nanoparticles. Int J Photoenergy 2018:1–7

Panchal P, Paul DR, Sharma A, Choudhary P, Meena P, Nehra SP (2020) Biogenic mediated Ag/ZnO nanocomposites for photocatalytic and antibacterial activities towards disinfection of water. J Colloid Interface Sci 563:370–380

Pascariu P, Homocianu M (2019) ZnO-based ceramic nanofibers: preparation, properties and applications. Ceram Int 45:11158–11173

Pascariu P, Cojocaru C, Samoila P, Airinei A, Suchea M (2020) Photocatalytic and antimicrobial activity of electrospun ZnO: Ag nanostructures. J Alloy Compd 834:155144–155154

Qi KZ, Xing XH, Zada A, Li MY, Wang Q, Liu SY, Lin HX, Wang GZ (2020) Transition metal doped ZnO nanoparticles with enhanced photocatalytic and antibacterial performances: experimental and DFT studies. Ceram Int 46:1494–1502

Quek JA, Lam SM, Mohamed AR (2018) Visible light responsive flower-like ZnO in photocatalytic antibacterial mechanism towards *Enterococcus faecalis* and *Micrococcus luteus*. J Photochem Photobiol B 187:66–75

Ray CAK (1999) Photocatalytic kinetics of phenol and its derivatives over UV irradiated $TiO_2$. Appl Catal B 23:143–157

Salah N, Al-Shawafi WM, Alshahrie A, Baghdadi N, Soliman YM, Memic A (2019) Size controlled, antimicrobial ZnO nanostructures produced by the microwave assisted route. Mater Sci Eng C 99:1164–1173

Salih FM (2010) Enhancement of solar inactivation of *Escherichia coli* by titanium dioxide photocatalytic oxidation. J Appl Microbiol 92:920–926

Sami R, Dionysiou DD, Pillai SC, John K (2018) Advances in catalytic/photocatalytic bacterial inactivation by nano Ag and Cu coated surfaces and medical devices. Appl Catal B 240:291–318

Sehar S, Naz I, Perveen I, Ahmed S (2019) Superior dye degradation using $SnO_2$-ZnO hybrid heterostructure catalysts. Korean J Chem Eng 36:56–62

Singh J, Dhaliwal AS (2020) Plasmon-induced photocatalytic degradation of methylene blue dye using biosynthesized silver nanoparticles as photocatalyst. Environ Technol 41:1520–1534

Thenmozhi S, Dharmaraj N, Kadirvelu K, Kim HY (2017) Electrospun nanofibers: new generation materials for advanced applications. Mater Sci Eng B 217:36–48

Vaiano V, Jaramillo-Paez CA, Matarangolo M, Navio J, Maria D (2019) UV and visible-light driven photocatalytic removal of caffeine using ZnO modified with different noble metals (Pt, Ag and Au). Mater Res Bull 112:251–260

Venkatesha TG, Nayaka YA, Viswanatha R, Vidyasagar CC, Chethana BK (2012) Electrochemical synthesis and photocatalytic behavior of flower shaped ZnO microstructures. Powder Technol 225:232–238

Wang T, Jiang Z, An T, Li G, Zhao H, Wong PK (2018) Enhanced visible-light-driven photocatalytic bacterial inactivation by ultrathin carbon-coated magnetic cobalt ferrite nanoparticles. Environ Sci Technol 52:4774–4784

Xia D, An T, Li G, Wang W, Zhao H, Wong PK (2016) Synergistic photocatalytic inactivation mechanisms of bacteria by graphene sheets grafted plasmonic Ag-AgX (X=Cl, Br, I) composite photocatalyst under visible light irradiation. Water Res 99:149–161

Yamanaka M, Hara K, Kudo J (2005) Bactericidal actions of a silver ion solution on *Escherichia coli*, studied by energy-filtering transmission electron microscopy and proteomic analysis. Appl Environ Microbiol 71:7589–7593

Yar A, Haspulat B, Üstün T, Eskizeybek V, Avcı A, Kamış H, Achour S (2017) Electrospun $TiO_2$/ZnO/PAN hybrid nanofiber membranes with efficient photocatalytic activity. RSC Adv 7:29806–29814

Yin WY, Weng YG, Jiang M, Yu SK, Zhu QY, Dai J (2020) A series of tetrathiafulvalene bismuth chlorides: effects of oxidation states of cations on structures and electric properties. Inorg Chem 59:5161–5169

Younis A, Chu D, Kaneti YV, Li S (2016) Tuning the surface oxygen concentration of 111 surrounded ceria nanocrystals for enhanced photocatalytic activities. Nanoscale 8:378–387

Younis A, Shirsath SE, Shabbir B, Li S (2018) Controllable dynamics of oxygen vacancies through extrinsic doping for superior catalytic activities. Nanoscale 10:18576–18585

Zhang C, Li Y, Zhang W, Wang P, Wang C (2017) Metal-free virucidal effects induced by g-C3N4 under visible light irradiation statistical analysis and parameter optimization. Chemosphere 195:551–558

Zhang BG, Zou SQ, Cai RQ, Li M, He Z (2018) Highly-efficient photocatalytic disinfection of *Escherichia coli* under visible light using carbon supported vanadium tetrasulfide nanocomposites. Appl Catal B Environ 224:383–393